



OPEN

# Effect of wear on the dynamic characteristics of a rigid rotor supported by journal bearings

Logamurthi Raja Moorthi<sup>1,2</sup>, Jawaid Iqbal Inayat-Hussain<sup>3,4✉</sup> & Azrul Abidin Zakaria<sup>3,5</sup>

The purpose of this work is to examine the effects of wear severity on the static and dynamic characteristics of journal bearings, and on the vibration response of a rigid rotor supported by journal bearings. Numerical simulations using MATLAB was conducted for three different operating regimes, namely low loaded operating regime ( $\epsilon_0 = 0.15$ ), moderately loaded operating regime ( $\epsilon_0 = 0.45$ ) and highly loaded operating regime ( $\epsilon_0 = 0.75$ ) with wear depth parameter ratio ( $\delta$ ) varied from 0 to 0.5 at increments of 0.1. Numerical results showed that the vibration response of the rotor generally increases with the increase of the wear depth for all cases of low, moderately and highly loaded operating regimes of the bearings. For the values of parameters considered in this work, it was shown that the vibration response amplitude of the rotor in worn journal bearings may be six times larger compared to the response amplitude of the rotor in non-worn bearings.

**Keywords** Rigid rotor, Wear, Dynamic coefficients, Journal bearing

Due to their superior long lasting and load carrying capacity, journal bearings are commonly utilized to support high-speed rotating machinery such as compressors and turbines<sup>1</sup>. However, the bearings are exposed to a gradual wear development amidst the rotating machine's operation, particularly during starts and stops or when passing through the rotor's critical speed<sup>2</sup>. As such, the bearing's geometry gets altered, thereby altering its dynamic characteristics<sup>3</sup>. Wear is amongst the most frequent failure that affects the bearing clearance at first hand and causes alterations to the rotating machine dynamics<sup>4</sup>. In the presence of wear, the pressure distribution, the rotor's equilibrium position, the bearing's dynamic coefficients and the system's response changes due to the alteration in oil film thickness<sup>5</sup>.

In rotor dynamics, the dynamics of hydrodynamic bearings are traditionally represented using stiffness and damping coefficients. Therefore, a linearization of hydrodynamic forces around the shaft's equilibrium position is required<sup>6</sup>. For that purpose, it is important to determine the forces created by the fluid flow to obtain precise estimates of the dynamics of the journal bearings. These forces can then be used to obtain the linearized stiffness and damping coefficients of the bearing. Linearized stiffness and damping coefficients are extensively utilized for rotor-bearing system's stability and response analyses. Pressure gradients are determined by a first order perturbation of the force and the linearized coefficients are estimated by employing numerical integration on the pressure gradients. Childs<sup>7</sup> as well as Yamamoto and Ishida<sup>8</sup> revealed a methodology to determine linearized coefficients for both the long bearing ( $L/D > 2$ ) and short bearing ( $L/D \leq 0.5$ ) approximations. Turaga et al.<sup>9</sup> employed a finite element method that accounts for the roughness on the bearing's surface to determine the bearing's linear coefficients. Rao and Sawicki<sup>10</sup> established a harmonic combination of the long and short bearings approximations (the inverse sum of the inverse of both pressures), initially proposed by Hirani et al.<sup>11</sup> to determine linearized coefficients for finite length bearings.

Several researchers have studied the behaviour of worn bearings utilized in rotating machines. Mokhtar et al.<sup>12</sup> experimentally examined the characteristic of wear in plain hydrodynamic journal bearings under repeated start and stop sequences. The wear was limited to the area where the shaft was known to slide on the bearing's surface during the early phases of the starting position; no wear was sustained while stopping since the shaft nearly stopped rotating before it made contact with the bearing. Dufrane et al.<sup>13</sup> examined the wear present in steam turbine bearings by taking measurements at predetermined time frames to determine the nature and extent of

<sup>1</sup>College of Graduate Studies, Universiti Tenaga Nasional, Jalan IKRAM-UNITEN, 43000 Kajang, Selangor, Malaysia. <sup>2</sup>Asset Operations and Maintenance, TNB Genco Sdn Bhd, Jalan Bangsar, 59200 Bangsar, Kuala Lumpur, Malaysia. <sup>3</sup>College of Engineering, Universiti Tenaga Nasional, Jalan IKRAM-UNITEN, 43000 Kajang, Selangor, Malaysia. <sup>4</sup>Institute of Power Engineering, Universiti Tenaga Nasional, Jalan IKRAM-UNITEN, 43000 Kajang, Selangor, Malaysia. <sup>5</sup>Institute of Sustainable Energy, Universiti Tenaga Nasional, Jalan IKRAM-UNITEN, 43000 Kajang, Selangor, Malaysia. ✉email: jawaid@uniten.edu.my

wear. For a more in-depth examination of the effect of wear on journal bearing, two wear geometry models were developed and utilized. Fillon et al.<sup>14</sup> studied the thermodynamic performance of a worn plain journal bearing. Because of its propensity to enter the wear-induced footprint, the worn bearing offers intriguing benefits like temperature drops. Bouyer et al.<sup>15</sup> presented an experimental data obtained on a journal lobed bearing subjected to numerous starts and stops. It was discovered that wear changes the properties of bearings, resulting in a decrease in temperature overall and an increase in maximum pressure. In their study, it is shown that, for the case investigated, while bearing characteristics is clearly affected by wear, the bearing still remains useable and safe.

Moreover, Machado et al.<sup>16</sup> developed a mathematical representation for the journal bearing's static analysis by utilizing the Reynolds equation. They acquired the pressure distribution in the bearing and examined the performance of dissimilar geometries in severe conditions, high speeds, and high-applied load. Chasalevris et al.<sup>17</sup> investigated the effect of worn journal bearings on the system response and specified the eventual development of additional frequency components. It was observed that sub- and superharmonics are revealed in the continuous wavelet transform (CWT) of the rotor-bearing system response for worn bearings. In the following year, Chasalevris et al.<sup>18</sup> designed and investigated an experimental rotor-bearing system with an elastic rotor mounted in worn journal bearings. The system is operated at run-up and run-down conditions and the response is analyzed with priority on passage through the first critical speed. When compared to the intact system, wear adds more sub- and super-harmonics to the response signal. Papanikolaou et al.<sup>5</sup> investigated the effect of wear of a short journal bearing on the rotordynamic stiffness and damping coefficients. Machado et al.<sup>2</sup> introduced a mathematical model to represent geometric discontinuities in journal bearing. They further presented a mathematical model that described the wear present in journal bearings and the effect of the wear on the dynamic response of the rotor-bearing system in frequency domain<sup>19</sup>. Jamil et al.<sup>20</sup> investigated the impact of wear in journal bearings on the dynamic behaviour of rotor bearing system relying upon the derivation of dynamic stiffness and damping coefficients of worn journal bearing. Kim et al.<sup>21</sup> presented a review that summarized the previous studies done on journal bearing induced nonlinear, rotordynamic forces, and responses. Viana et al.<sup>6</sup> investigated the boundaries for linear approximation of the hydrodynamic forces present in lobed hydrodynamic bearings in highly loaded operating conditions.

Whenever there is a change in the clearance of the bearing due to wear, the characteristics such as the static equilibrium position and the linearized dynamic coefficient will change. This will affect the vibration response of the rotor supported by the worn bearings. The purpose of the present paper is therefore to examine the effect of wear on the vibration response of a rigid rotor supported by worn bearings. In this paper, the wear model proposed by Dufrane et al.<sup>13</sup> is used in the mathematical model of a short journal bearing. The oil film forces acting on the rotor and the dynamic coefficients (stiffness and damping) are computed for both cases of bearing without wear and bearing with wear. The dynamic coefficients are computed for different wear depth, and these coefficients are then used to determine the vibration response of a rigid rotor.

## Mathematical treatment

### Wear model

The wear model used in this paper is the model proposed by Dufrane et al.<sup>13</sup> and it is shown schematically in Fig. 1<sup>5</sup>. The region of positive pressure in the state of worn journal bearing can be divided into three sub regions<sup>20</sup>. The derivation of the equation presented herein follows the work of Papanikolaou et al.<sup>5</sup> and Jamil et al.<sup>20</sup>.

1<sup>st</sup> Non-worn region ( $0 \leq \theta \leq \theta_s$ )

In the 1<sup>st</sup> non-worn region, the fluid-film thickness,  $h_0$ , is expressed by Eq. (1).

$$h_0 = C + e_0 \cos \theta \quad (1)$$

where,

$h_0$  is the fluid film thickness in the non-worn region (m).

$C$  is the radial clearance (m).

$e_0$  is the eccentricity between the journal center and bearing center at equilibrium position (m).

$\theta$  is the angular coordinate measured from the position of maximum fluid-film thickness in the direction of rotor angular velocity (counter-clockwise), (rad).

For small amplitude motions about the journal equilibrium position, the fluid-film thickness,  $h$ , can be rewritten as shown in the following equation:

$$h = C + e(t) \cos \theta \quad (2)$$

where,

$h$  is the fluid-film thickness for small amplitude motions about the journal equilibrium position (m).

$\theta = \gamma - \varphi_0$ ;  $\gamma$  is the angle measured from the vertical axis,  $X$ , in the direction of rotor angular velocity (counter-clockwise), (rad).

$\varphi_0$  is the attitude angle measured from the vertical axis,  $X$ , to the position of maximum fluid-film thickness in the direction of rotor angular velocity (counter-clockwise), (rad).

The time-dependent eccentricity  $e(t)$  and attitude angle  $\varphi(t)$  are given by:

$$\begin{aligned} e(t) &= e_0 + \Delta e(t) \\ \varphi(t) &= \varphi_0 + \Delta \varphi_0 \end{aligned} \quad (3)$$

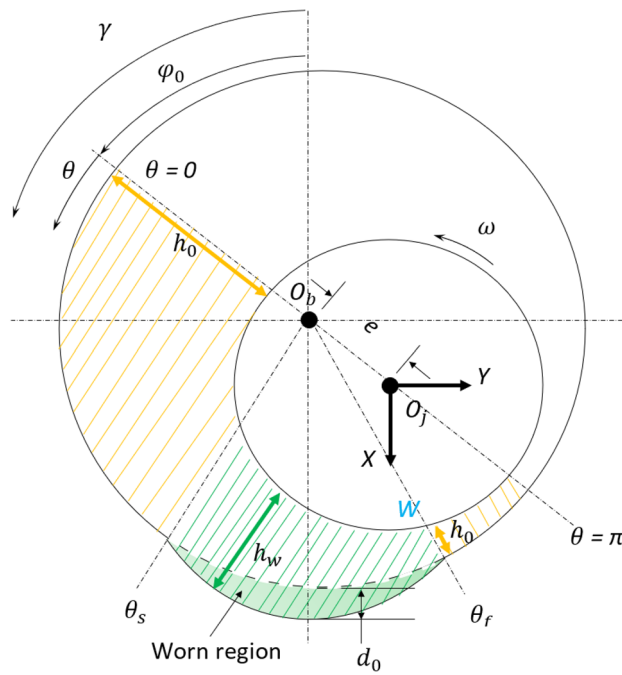


**Figure 1.** Wear model<sup>5</sup>.

$\Delta e$  and  $\Delta \varphi$  are small radial displacement and small variation of attitude angle respectively. Substituting Eq. (3) into Eq. (2) yields:

$$h = C + (e_0 + \Delta e)\cos\theta\cos\Delta\varphi + \sin\theta\sin\Delta\varphi \tag{4}$$

For small amplitude of motion, the following relationship is valid.

$$\begin{aligned} \cos\Delta\varphi &\sim 1; \\ \sin\Delta\varphi &\sim \Delta\varphi; \\ \Delta e\Delta\varphi &= 0 \end{aligned} \tag{5}$$

Substituting Eq. (5) into Eq. (4) gives the following expression for the instantaneous fluid-film thickness in the non-worn region.

$$h = C + e_0\cos\theta + \Delta e\cos\theta + e_0\Delta\varphi\sin\theta \tag{6}$$

Differentiating Eq. (6) with respect to  $\theta$  results in Eq. (7), which describes the change of fluid-film thickness in the circumferential direction of the bearing.

$$\frac{\partial h}{\partial \theta} = -e_0\sin\theta - \Delta e\sin\theta + e_0\Delta\varphi\cos\theta \tag{7}$$

Differentiating Eq. (6) with respect to time,  $t$ , results in Eq. (8), which describes the change, with time, of the fluid-film thickness at a fixed point in the bearing.

$$\frac{\partial h}{\partial t} = \Delta \dot{e}\cos\theta + e_0\Delta\dot{\varphi}\sin\theta \tag{8}$$

Worn region ( $\theta_s \leq \theta \leq \theta_f$ )

In the worn region, the fluid-film thickness,  $h_{0w}$ , is expressed by Eq. (9).

$$h_{0w} = d_0 + e_0\cos\theta - C\cos(\theta + \varphi_0) \tag{9}$$

where,

$h_{0w}$  is the worn fluid film thickness at equilibrium position (m);

$C$  is the journal bearing radial clearance (m).

$d_0$  is the wear depth (m).

Substituting Eq. (3) into Eq. (9) yields:

$$h_w = d_0 + (e_0 + \Delta e) \cos(\gamma - \varphi_0 - \Delta \varphi) - C \cos(\theta + \varphi_0) \quad (10)$$

Substituting Eq. (5) into Eq. (10) gives the following expression for the instantaneous fluid-film thickness in worn region.

$$h_w = d_0 + e_0 \cos \theta - C \cos(\theta + \varphi_0) + e_0 \Delta \varphi \sin \theta + \Delta e \cos \theta \quad (11)$$

Differentiating Eq. (11) with respect to  $\theta$  yields Eq. (12), which describes the change of fluid-film thickness in the circumferential direction of the bearing.

$$\frac{\partial h_w}{\partial \theta} = C \sin(\theta + \varphi_0) - e_0 \sin \theta - \Delta e \sin \theta + e_0 \Delta \varphi \cos \theta \quad (12)$$

Differentiating Eq. (11) with respect to time,  $t$ , yields Eq. (13), which describes the change, with time, of the fluid-film thickness at a fixed point in the bearing.

$$\frac{\partial h_w}{\partial t} = \Delta \dot{e} \cos \theta + e_0 \Delta \dot{\varphi} \sin \theta \quad (13)$$

### 2<sup>nd</sup> Non-worn region ( $\theta_f \leq \theta \leq \pi$ )

In this region the thickness of lubricant oil fluid is as in the 1<sup>st</sup> non-worn region. The starting and final angles of the region where the wear takes place (refer to Fig. 1) are given by:

$$\cos(\theta + \varphi_0) = \frac{d_0}{c} - 1 = \delta - 1 \quad (14)$$

where,

$$\delta = \frac{d_0}{c},$$

$\delta$  is the wear depth parameter.

$\theta_s$  and  $\theta_f$  are represented by the following equations<sup>20</sup>:

$$\theta_s = \pi - \varphi_0 - \arccos(1 - \delta) \quad (15)$$

$$\theta_f = \pi - \varphi_0 + \arccos(1 - \delta) \quad (16)$$

## Solution to bearing forces and dynamic coefficients

The fluid film pressure is obtained by solving the Reynolds equation for infinitely short bearing ( $L/D < 0.5$ ). The bearing forces are computed by integrating the fluid film pressure over the bearing area using Simpson's 1/3 rule.

### Reynolds equation

For convenience purposes, polar coordinates is employed instead of Cartesian coordinates to solve the Reynolds equation. The polar coordinates used are the eccentricity ratio,  $\epsilon_0$  and the attitude angle  $\varphi_0$ .

With the following assumptions: (i) short journal bearing, (ii) laminar fluid flow, (iii) iso-viscous fluid, (iv) incompressible fluid, and (v)  $\pi$ -film cavitation model, the Reynolds equation is written as follows<sup>20</sup>:

$$\frac{\partial}{\partial Z} \left( \frac{h^3}{12\mu} \frac{\partial P}{\partial Z} \right) = \frac{\partial h}{\partial t} + \frac{\Omega}{2} \frac{\partial h}{\partial \theta} \quad (17)$$

where,

$\Omega$  is the rotational speed of the rotor (rad/s)

$\mu$  is the fluid viscosity (Pa.s)

By integrating the Reynolds equation with respect to  $Z$ , the pressure distribution for the non-worn and worn regions are obtained<sup>20</sup>:

Non-worn region: The pressure distribution in the non-worn region,  $P$ , is expressed by Eq. (18).

$$P(\theta, Z, t) = \frac{6\mu}{h^3} \left( \frac{\partial h}{\partial t} + \frac{\Omega}{2} \frac{\partial h}{\partial \theta} \right) \left( Z^2 - \frac{L^2}{4} \right) \quad (18)$$

where,

$L$  is the journal bearing length (m).

$Z$  is the axial distance in the direction of  $Z$ -axis

Worn region: The pressure distribution in the worn region,  $P_w$ , is expressed by Eq. (19).

$$P_w(\theta, Z, t) = \frac{6\mu}{h^3} \left( \frac{\partial h_w}{\partial t} + \frac{\Omega}{2} \frac{\partial h_w}{\partial \theta} \right) \left( Z^2 - \frac{L^2}{4} \right) \quad (19)$$

where,

$P_w$  is the pressure in the worn region of the journal bearing;

$h_w$  is the fluid film thickness in the worn region of the journal bearing.

*Dynamic coefficients of worn journal bearings*

The radial and tangential components of fluid film journal bearing forces are presented in Eq. (20)<sup>20</sup>:

$$\begin{Bmatrix} F_r \\ F_t \end{Bmatrix} = 2 \int_0^{L/2} \int_0^\pi P(\theta, Z, t) R \begin{pmatrix} \cos\theta \\ \sin\theta \end{pmatrix} d\theta dz \quad (20)$$

Substituting the equation for pressure distribution in the non-worn regions and worn region of fluid film journal bearing into Eq. (20) gives:

$$\begin{aligned} \begin{Bmatrix} F_r \\ F_t \end{Bmatrix} &= \frac{12\mu}{h^3} R \int_0^{L/2} \left\{ \int_0^{\theta_s} \left( \frac{\partial h}{\partial t} + \frac{\Omega}{2} \frac{\partial h}{\partial \theta} \right) + \int_{\theta_s}^{\theta_f} \left( \frac{\partial h_w}{\partial t} + \frac{\Omega}{2} \frac{\partial h_w}{\partial \theta} \right) \right. \\ &\quad \left. + \int_{\theta_f}^\pi \left( \frac{\partial h}{\partial t} + \frac{\Omega}{2} \frac{\partial h}{\partial \theta} \right) \right\} \begin{pmatrix} \cos\theta \\ \sin\theta \end{pmatrix} \left( Z^2 - \frac{L^2}{4} \right) d\theta dz \end{aligned} \quad (21)$$

Substituting Eq. (21) with Eqs. (7), (8), (12) and (13) and integrating the result with respect to Z gives the following expression:

$$\begin{aligned} \begin{Bmatrix} F_r \\ F_t \end{Bmatrix} &= -\frac{\Omega}{2} \frac{\mu L^3 R}{c^3 H^3} \int_0^{\theta_s} \begin{Bmatrix} -e_0 \sin\theta \cos\theta \\ -e_0 \sin^2\theta \end{Bmatrix} d\theta - \frac{\Omega}{2} \frac{\mu L^3 R}{c^3 H^3} \int_{\theta_f}^\pi \begin{Bmatrix} -e_0 \sin\theta \cos\theta \\ -e_0 \sin^2\theta \end{Bmatrix} d\theta \\ &\quad - \frac{\Omega}{2} \frac{\mu L^3 R}{c^3 H_w^3} \int_{\theta_s}^{\theta_f} \begin{Bmatrix} -e_0 \sin\theta \cos\theta + c \sin(\theta + \varphi_0) \cos\theta \\ -e_0 \sin^2\theta \end{Bmatrix} d\theta \\ &\quad - \frac{\Omega}{2} \frac{\mu L^3 R}{c^3 H^3} \left[ \int_0^{\theta_s} \begin{Bmatrix} -\sin\theta \cos\theta \\ -\sin^2\theta \end{Bmatrix} d\theta \right] \Delta e - \frac{\Omega}{2} \frac{\mu L^3 R}{c^3 H^3} \left[ \int_0^{\theta_s} \begin{Bmatrix} \cos^2\theta \\ \sin\theta \cos\theta \end{Bmatrix} d\theta \right] e_0 \Delta \varphi \\ &\quad - \frac{\Omega}{2} \frac{\mu L^3 R}{c^3 H_w^3} \left[ \int_{\theta_s}^{\theta_f} \begin{Bmatrix} -\sin\theta \cos\theta \\ -\sin^2\theta \end{Bmatrix} d\theta \right] \Delta e - \frac{\Omega}{2} \frac{\mu L^3 R}{c^3 H_w^3} \left[ \int_{\theta_s}^{\theta_f} \begin{Bmatrix} \cos^2\theta \\ \sin\theta \cos\theta \end{Bmatrix} d\theta \right] e_0 \Delta \varphi \\ &\quad - \frac{\Omega}{2} \frac{\mu L^3 R}{c^3 H^3} \left[ \int_{\theta_f}^\pi \begin{Bmatrix} -\sin\theta \cos\theta \\ -\sin^2\theta \end{Bmatrix} d\theta \right] \Delta e - \frac{\Omega}{2} \frac{\mu L^3 R}{c^3 H^3} \left[ \int_{\theta_f}^\pi \begin{Bmatrix} \cos^2\theta \\ \sin\theta \cos\theta \end{Bmatrix} d\theta \right] e_0 \Delta \varphi \\ &\quad - \frac{\Omega}{2} \frac{\mu L^3 R}{c^3 H^3} \left[ \int_0^{\theta_s} \begin{Bmatrix} \cos^2\theta \\ \sin\theta \cos\theta \end{Bmatrix} d\theta \right] \Delta \dot{e} - \frac{\Omega}{2} \frac{\mu L^3 R}{c^3 H^3} \left[ \int_0^{\theta_s} \begin{Bmatrix} \sin\theta \cos\theta \\ \sin^2\theta \end{Bmatrix} d\theta \right] e_0 \Delta \dot{\varphi} \\ &\quad - \frac{\Omega}{2} \frac{\mu L^3 R}{c^3 H_w^3} \left[ \int_{\theta_s}^{\theta_f} \begin{Bmatrix} \cos^2\theta \\ \sin\theta \cos\theta \end{Bmatrix} d\theta \right] \Delta \dot{e} - \frac{\Omega}{2} \frac{\mu L^3 R}{c^3 H_w^3} \left[ \int_{\theta_s}^{\theta_f} \begin{Bmatrix} \sin\theta \cos\theta \\ \sin^2\theta \end{Bmatrix} d\theta \right] e_0 \Delta \dot{\varphi} \\ &\quad - \frac{\Omega}{2} \frac{\mu L^3 R}{c^3 H^3} \left[ \int_{\theta_f}^\pi \begin{Bmatrix} \cos^2\theta \\ \sin\theta \cos\theta \end{Bmatrix} d\theta \right] \Delta \dot{e} - \frac{\Omega}{2} \frac{\mu L^3 R}{c^3 H^3} \left[ \int_{\theta_f}^\pi \begin{Bmatrix} \sin\theta \cos\theta \\ \sin^2\theta \end{Bmatrix} d\theta \right] e_0 \Delta \dot{\varphi} \end{aligned} \quad (22)$$

where,

$$H = \frac{h}{c} \text{ and } H_w = \frac{h_w}{c}$$

The solution of Eq. (22) has the following form<sup>22</sup>:

$$\begin{Bmatrix} F_r \\ F_t \end{Bmatrix} = \begin{Bmatrix} F_{r0} \\ F_{t0} \end{Bmatrix} - \begin{bmatrix} K_{rr} & K_{rt} \\ K_{tr} & K_{tt} \end{bmatrix} \begin{bmatrix} \Delta e \\ e_0 \Delta \varphi \end{bmatrix} - \begin{bmatrix} C_{rr} & C_{rt} \\ C_{tr} & C_{tt} \end{bmatrix} \begin{bmatrix} \Delta \dot{e} \\ e_0 \Delta \dot{\varphi} \end{bmatrix} \quad (23)$$

Simpsons 1/3 rule is used to solve Eq. (23) and the solution can be described as:

$$\begin{aligned}
F_{r0} &= c.F_s \left\{ \int_0^{\theta_s} \frac{\epsilon_0 \sin\theta \cos\theta}{H_0^3} d\theta + \int_{\theta_s}^{\theta_f} \frac{\epsilon_0 \sin\theta \cos\theta - \cos\theta \sin(\theta + \varphi_0)}{H_{0w}^3} d\theta \right. \\
&\quad \left. + \int_{\theta_f}^{\pi} \frac{\epsilon_0 \sin\theta \cos\theta}{H_0^3} d\theta \right\} \\
F_{t0} &= c.F_s \left\{ \int_0^{\theta_s} \frac{\epsilon_0 (\sin\theta)^2}{H_0^3} d\theta + \int_{\theta_s}^{\theta_f} \frac{\epsilon_0 (\sin\theta)^2 - \sin\theta \sin(\theta + \varphi_0)}{H_{0w}^3} d\theta \right. \\
&\quad \left. + \int_{\theta_f}^{\pi} \frac{\epsilon_0 (\sin\theta)^2}{H_0^3} d\theta \right\} \\
K_{rr} &= F_s \left\{ - \int_0^{\theta_s} \frac{\sin\theta \cos\theta}{H_0^3} d\theta + 3.\epsilon_0. \int_0^{\theta_s} \frac{\sin\theta (\cos\theta)^2}{H_0^4} d\theta \right. \\
&\quad - \int_{\theta_s}^{\theta_f} \frac{\sin\theta \cos\theta}{H_{0w}^3} d\theta + 3.\epsilon_0. \int_{\theta_s}^{\theta_f} \frac{\sin\theta (\cos\theta)^2}{H_{0w}^4} d\theta \\
&\quad - 3. \int_{\theta_s}^{\theta_f} \frac{(\cos\theta)^2 \sin(\theta + \varphi_0)}{H_{0w}^4} d\theta - \int_{\theta_f}^{\pi} \frac{\sin\theta \cos\theta}{H_0^3} d\theta \\
&\quad \left. + 3.\epsilon_0. \int_{\theta_f}^{\pi} + \frac{\sin\theta (\cos\theta)^2}{H_0^4} d\theta \right\} \\
K_{rt} &= F_s \left\{ \int_0^{\theta_s} \frac{(\cos\theta)^2}{H_0^3} d\theta + 3.\epsilon_0. \int_0^{\theta_s} \frac{\cos\theta (\sin\theta)^2}{H_0^4} d\theta \right. \\
&\quad + 3.\epsilon_0. \int_{\theta_s}^{\theta_f} \frac{(\sin\theta)^2 \cos\theta}{H_{0w}^4} d\theta + \int_{\theta_s}^{\theta_f} \frac{(\cos\theta)^2}{H_{0w}^3} d\theta \\
&\quad - 3. \int_{\theta_s}^{\theta_f} \frac{\cos\theta \sin(\theta + \varphi_0)}{H_{0w}^4} d\theta + \int_{\theta_f}^{\pi} \frac{(\cos\theta)^2}{H_0^3} d\theta \\
&\quad \left. + 3.\epsilon_0. \int_{\theta_f}^{\pi} + \frac{\cos\theta (\sin\theta)^2}{H_0^4} d\theta \right\} \\
K_{tr} &= F_s \left\{ - \int_0^{\theta_s} \frac{(\sin\theta)^2}{H_0^3} d\theta + 3.\epsilon_0. \int_0^{\theta_s} \frac{\cos\theta (\sin\theta)^2}{H_0^4} d\theta \right. \\
&\quad + 3.\epsilon_0. \int_{\theta_s}^{\theta_f} \frac{(\sin\theta)^2 \cos\theta}{H_{0w}^4} d\theta - \int_{\theta_s}^{\theta_f} \frac{(\sin\theta)^2}{H_{0w}^3} d\theta \\
&\quad - 3. \int_{\theta_s}^{\theta_f} \frac{\sin\theta \cos\theta \sin(\theta + \varphi_0)}{H_{0w}^4} d\theta - \int_{\theta_f}^{\pi} \frac{(\sin\theta)^2}{H_0^3} d\theta \\
&\quad \left. + 3.\epsilon_0. \int_{\theta_f}^{\pi} + \frac{\cos\theta (\sin\theta)^2}{H_0^4} d\theta \right\} \\
K_{tt} &= F_s \left\{ \int_0^{\theta_s} \frac{\sin\theta \cos\theta}{H_0^3} d\theta + 3.\epsilon_0. \int_0^{\theta_s} \frac{(\sin\theta)^3}{H_0^4} d\theta \right. \\
&\quad + 3.\epsilon_0. \int_{\theta_s}^{\theta_f} \frac{(\sin\theta)^3}{H_{0w}^4} d\theta + \int_{\theta_s}^{\theta_f} \frac{\sin\theta \cos\theta}{H_{0w}^3} d\theta \\
&\quad - 3. \int_{\theta_s}^{\theta_f} \frac{(\sin\theta)^2 \sin(\theta + \varphi_0)}{H_{0w}^4} d\theta + \int_{\theta_f}^{\pi} \frac{\sin\theta \cos\theta}{H_0^3} d\theta \\
&\quad \left. + 3.\epsilon_0. \int_{\theta_f}^{\pi} + \frac{(\sin\theta)^3}{H_0^4} d\theta \right\} \\
C_{rr} &= \frac{2F_s}{\Omega} \left\{ \int_0^{\theta_s} \frac{(\cos\theta)^2}{H_0^3} d\theta + \int_{\theta_s}^{\theta_f} \frac{(\cos\theta)^2}{H_{0w}^3} d\theta + \int_{\theta_f}^{\pi} \frac{(\cos\theta)^2}{H_0^3} d\theta \right\} \\
C_{rt} &= \frac{2F_s}{\Omega} \left\{ \int_0^{\theta_s} \frac{\sin\theta \cos\theta}{H_0^3} d\theta + \int_{\theta_s}^{\theta_f} \frac{\sin\theta \cos\theta}{H_{0w}^3} d\theta + \int_{\theta_f}^{\pi} \frac{\sin\theta \cos\theta}{H_0^3} d\theta \right\} \\
C_{tr} &= \frac{2F_s}{\Omega} \left\{ \int_0^{\theta_s} \frac{\sin\theta \cos\theta}{H_0^3} d\theta + \int_{\theta_s}^{\theta_f} \frac{\sin\theta \cos\theta}{H_{0w}^3} d\theta + \int_{\theta_f}^{\pi} \frac{\sin\theta \cos\theta}{H_0^3} d\theta \right\} \\
C_{tt} &= \frac{2F_s}{\Omega} \left\{ \int_0^{\theta_s} \frac{(\sin\theta)^2}{H_0^3} d\theta + \int_{\theta_s}^{\theta_f} \frac{(\sin\theta)^2}{H_{0w}^3} d\theta + \int_{\theta_f}^{\pi} \frac{(\sin\theta)^2}{H_0^3} d\theta \right\}
\end{aligned} \tag{24}$$

where,

$$F_s = \frac{\mu\Omega RL^3}{2c^3}$$

The dynamic coefficients  $K_{ij}$  and  $C_{ij}$  refer to the rotating coordinate system and not to the Cartesian coordinate system. The relationship between the dynamic coefficients in both coordinate systems can be determined by the following transformations<sup>5</sup>:

$$\begin{aligned} \begin{bmatrix} K_{yx} & K_{xy} \\ K_{yx} & K_{yy} \end{bmatrix} &= \begin{bmatrix} \cos\varphi_0 & -\sin\varphi_0 \\ \sin\varphi_0 & \cos\varphi_0 \end{bmatrix} \begin{bmatrix} K_{rr} & K_{rt} \\ K_{tr} & K_{tt} \end{bmatrix} \begin{bmatrix} \cos\varphi_0 & \sin\varphi_0 \\ -\sin\varphi_0 & \cos\varphi_0 \end{bmatrix} \\ \begin{bmatrix} C_{yx} & C_{xy} \\ C_{yx} & C_{yy} \end{bmatrix} &= \begin{bmatrix} \cos\varphi_0 & -\sin\varphi_0 \\ \sin\varphi_0 & \cos\varphi_0 \end{bmatrix} \begin{bmatrix} C_{rr} & C_{rt} \\ C_{tr} & C_{tt} \end{bmatrix} \begin{bmatrix} \cos\varphi_0 & \sin\varphi_0 \\ -\sin\varphi_0 & \cos\varphi_0 \end{bmatrix} \end{aligned} \tag{25}$$

For the worn journal bearing, the attitude angle  $\varphi_0$  can be determined from Eq. (26)

$$\tan^{-1}\varphi_0 = -\frac{F_{t0}}{F_{r0}} \tag{26}$$

However, in the case of non-worn bearing,  $\varphi_0$  can be related to  $\epsilon_0$ , by the following expression<sup>22</sup>.

$$\tan^{-1}\varphi_0 = -\frac{\pi\sqrt{(1-\epsilon_0^2)}}{4\epsilon_0} \tag{27}$$

### Equation of motion of a rigid rotor in journal bearing

In the formulation of the equations of motion, the rotor is assumed to be rigid, symmetric and with a centrally-located mass. Therefore, only the lowest mode (cylindrical) can be excited by the applied unbalance. Rotor motion in the axial direction is neglected, and only the motion in the vertical (X) and horizontal (Y) directions are considered in the formulation of the equations of motion. Let the rotor mass be  $2M$  and the journal center amplitudes  $\bar{x}$  and  $\bar{y}$ . Hence, the equations of motion can be written<sup>22</sup>:

$$\begin{aligned} M\frac{d^2\bar{x}}{dt^2} &= F_x + MU\omega^2\cos\omega t \\ M\frac{d^2\bar{y}}{dt^2} &= F_y + MU\omega^2\sin\omega t \end{aligned} \tag{28}$$

Here  $F_x$  and  $F_y$  are the journal bearing film forces. The equations are made dimensionless by setting<sup>23</sup>:

$$\begin{aligned} x &= \frac{\bar{x}}{C}; y = \frac{\bar{y}}{C}; u = \frac{\bar{U}}{C}; \tau = \omega t \\ f_x &= \frac{1}{\sigma} \frac{F_x}{W} \\ f_y &= \frac{1}{\sigma} \frac{F_y}{W} \\ m &= \frac{1}{\sigma} \frac{CM\omega^2}{W} \end{aligned} \tag{29}$$

where modified Sommerfeld number:

$$\sigma = \frac{1}{8} \frac{\mu\omega DL}{W} \left(\frac{L}{C}\right)^2 \tag{30}$$

$\mu$  is the lubricant viscosity,  $\omega$  is the angular speed,  $D$  is the bearing diameter,  $L$  is the bearing length,  $W$  is the static load on the bearing,  $C$  is the radial bearing clearance.

The modified Sommerfeld number,  $\sigma$ , can be related to the eccentricity ratio,  $\epsilon_0$ , by the following expression.

$$\sigma = \frac{(1-\epsilon_0^2)^2}{\epsilon_0\sqrt{16\epsilon_0^2 + \pi^2(1-\epsilon_0^2)}} \tag{31}$$

Letting “dot” refer to  $d/d\tau$  and substituting Eq. (29) into Eq. (28), the dimensionless equations of motion become:

$$\begin{aligned} m\ddot{x} &= f_x + mu\omega^2\cos\tau \\ m\ddot{y} &= f_y + mu\omega^2\sin\tau \end{aligned} \tag{32}$$

where,

$$\begin{aligned} f_x &= -K_{xx}x - K_{xy}y - C_{xx}\dot{x} - C_{xy}\dot{y} \\ f_y &= -K_{yy}y - K_{yx}x - C_{yx}\dot{x} - C_{yy}\dot{y} \end{aligned}$$

Hence, Eq. (32) can be written in the following form:

$$\begin{bmatrix} m & 0 \\ 0 & m \end{bmatrix} \begin{bmatrix} \ddot{x} \\ \ddot{y} \end{bmatrix} + \begin{bmatrix} C_{xx} & C_{xy} \\ C_{yx} & C_{yy} \end{bmatrix} \begin{bmatrix} \dot{x} \\ \dot{y} \end{bmatrix} + \begin{bmatrix} K_{xx} & K_{xy} \\ K_{yx} & K_{yy} \end{bmatrix} \begin{bmatrix} x \\ y \end{bmatrix} = \begin{bmatrix} \mu\omega^2 \cos\tau \\ \mu\omega^2 \sin\tau \end{bmatrix} \quad (33)$$

Eq. (33) is solved for  $x$  and  $y$  using MATLAB linear solver.

## Results and discussion

### Effect of wear on the static equilibrium position

The effect of wear on the static equilibrium position was examined for values of  $\epsilon_0$  between 0.1 and 0.9. The wear depth parameter ratio  $\delta$  was varied from 0 to 0.5, in increments of 0.1. Figure 2a shows the relationship between  $\varphi_0$  and  $\epsilon_0$  for bearing without wear. It is observed that  $\epsilon_0$  has an inverse relationship with  $\varphi_0$  whereby that  $\epsilon_0$  increases as  $\varphi_0$  decreases. To understand the relationship between  $\varphi_0$  and  $\epsilon_0$ , the relationship between  $\sigma$  and  $\epsilon_0$  needs to be understood first as expressed in Eq. (31). Equation (31) provides a relationship to determine  $\epsilon_0$  required to generate the fluid film reaction force. Large  $\sigma$  represents low operating load, high  $\omega$  or high fluid viscosity,  $\mu$ , which results in small  $\epsilon_0$  or nearly centered operation,  $\epsilon_0 \rightarrow 0, \varphi_0 \rightarrow \pi/2$ . That is, the journal eccentricity vector is nearly orthogonal to the applied load. Small  $\sigma$  represents high operating load, low  $\omega$  or small  $\mu$ , which results in large  $\epsilon_0, \epsilon_0 \rightarrow 1.0, \varphi_0 \rightarrow 0$ . That is, the journal eccentricity vector is nearly parallel to the applied load. The relationship between  $\varphi_0$  and  $\epsilon_0$  is expressed in Eq. (27) and this equation is only valid to calculate  $\varphi_0$  for the case of bearing without wear. However, for the case of worn bearing,  $\varphi_0$  is calculated iteratively using Eq. (26)<sup>22</sup>.

Figure 2b shows the relationship between  $\varphi_0$  and  $\epsilon_0$  for worn bearing. The variation of  $\varphi_0$  is demonstrated as a function of  $\epsilon_0$  and  $\delta$ . It is observed that, for a constant value of  $\epsilon_0$ ,  $\varphi_0$  decreases as  $\delta$  increases. For example,  $\epsilon_0$  is set constant at 0.01 and  $\delta$  is varied from 0 to 0.5. When  $\delta = 0, \varphi_0 = 1.558$  and when  $\delta = 0.5, \varphi_0 = 1.111$ , giving a percentage difference of 28.72% between a non-worn and worn bearing. Moreover, the percentage difference between a non-worn and worn bearing also increases as  $\epsilon_0$  increases<sup>24</sup>. For example,  $\epsilon_0$  is set constant at 0.7 and

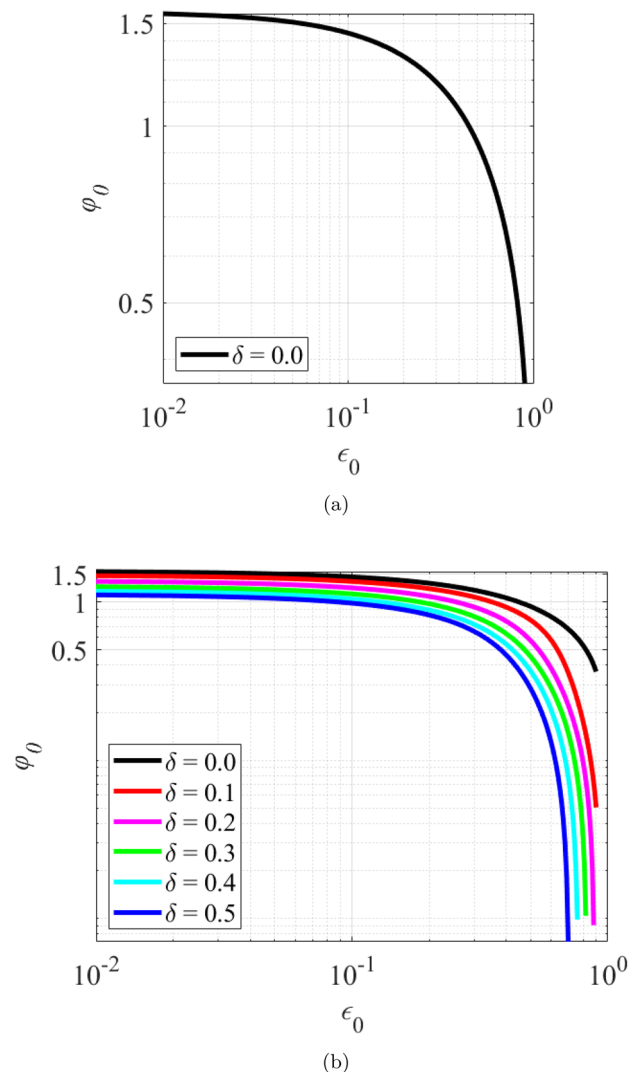


**Figure 2.** Relationship between  $\epsilon_0$  and  $\varphi_0$  for (a) bearing without wear (b) worn bearing.



$\delta$  is varied from 0 to 0.5. When  $\delta = 0$ ,  $\varphi_0 = 0.676$  and when  $\delta = 0.5$ ,  $\varphi_0 = 0.007$ , calculating a percentage difference of 98.95% between a non-worn and worn bearing. The static equilibrium position from the present work in the condition when there is no wear ( $\delta = 0$ ) matches closely to those that were presented by Jamil et al.<sup>20</sup>

The fluid film thickness in the journal bearing, given in Eqs. (1) and (9), respectively for the non-worn and worn journal bearing, is a function of the attitude angle  $\varphi_0$ . For a given value of  $\epsilon_0$ , the attitude angle varies with the depth of wear, as illustrated in Fig. 2b. Therefore, the angular position ( $\gamma$ ) where the minimum film thickness occurs changes with the depth of wear. The fluid film thickness profile for the case of  $\epsilon_0=0.4$  is shown in Fig. 3 for various wear depth values. It is observed that as the wear depth increases, the angular position ( $\gamma$ ) where the minimum film thickness occurs decreases.

### Effect of wear on the dynamic coefficients of journal bearings

The effect of wear on the dynamic coefficients of journal bearings was investigated for values of  $\epsilon_0$  between 0.1 and 0.75. The wear depth parameter ratio  $\delta$  was varied from 0 to 0.5. Figures 4 and 5 show the dimensionless stiffness and damping coefficient as a function of  $\sigma$  for (a) bearing with  $\delta = 0$  (b) bearing with  $\delta = 0.5$ . It is observed that wear alters the relation between the direct and the cross coupled stiffness coefficients in both the X-direction and the Y-direction, especially at low  $\sigma$ . As reported by Machado and Cavalca<sup>19</sup>, the wear increases the anisotropic characteristics of these coefficients. The dimensionless linearized dynamic coefficient from the present work in the condition when there is no wear ( $\delta = 0$ ) closely matches those that were presented by Jamil et al.<sup>20</sup>

Figure 6 shows the dimensionless dynamic stiffness coefficient against  $\delta$  ranging from  $\delta = 0$  to  $\delta = 0.5$  when the rotor is operated under high operating regime ( $\epsilon_0 = 0.61$ ). It is observed that  $K_{xx}$  increases by 38.37%,  $K_{xy}$  reduces by 51.25%,  $K_{yx}$  reduces by 309.72%, and  $K_{yy}$  reduces by 75.46%.

Dynamic direct stiffness coefficient relates the change in force in one direction to a displacement in the same direction as shown in Eqs. (34) and (35)<sup>25</sup>:

$$K_{xx} = \frac{\Delta F_x}{\Delta x} \quad (34)$$

$$K_{yy} = \frac{\Delta F_y}{\Delta y} \quad (35)$$

The nature of the dynamic direct stiffness is to provide a restoring force that pushes the journal back toward its steady-state equilibrium position<sup>25</sup>. In Fig. 6, it is seen that the dynamic direct stiffness coefficients  $K_{yy}$  decreases with increasing  $\delta$  whereas the direct stiffness coefficient  $K_{xx}$  increases with increasing  $\delta$ . This is because when  $\delta$  increases,  $\varphi_0$  decreases and  $\epsilon_0$  increases which causes the rotor to move closer to the X-axis and further in the X-direction. As such, the displacement in the X-direction,  $\Delta x$  and the restoring force in the X-direction,  $\Delta F_x$ , increases whereas the displacement in the Y-direction,  $\Delta y$ , and the restoring force in the Y-direction,  $\Delta F_y$ , reduces. As a result, an increase in  $K_{xx}$  and a drop in  $K_{yy}$  is observed.

The cross-coupled stiffness relates to a displacement resulted in force component perpendicular to this displacement as given in Eqs. (36) and (37)<sup>25</sup>:

$$K_{xy} = \frac{\Delta F_x}{\Delta y} \quad (36)$$

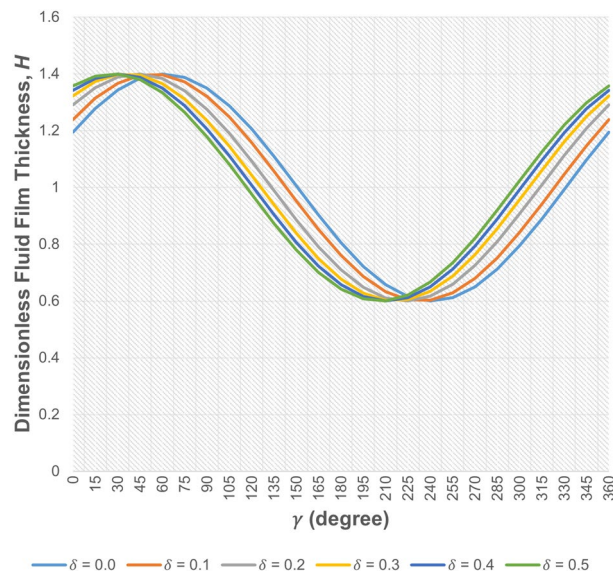
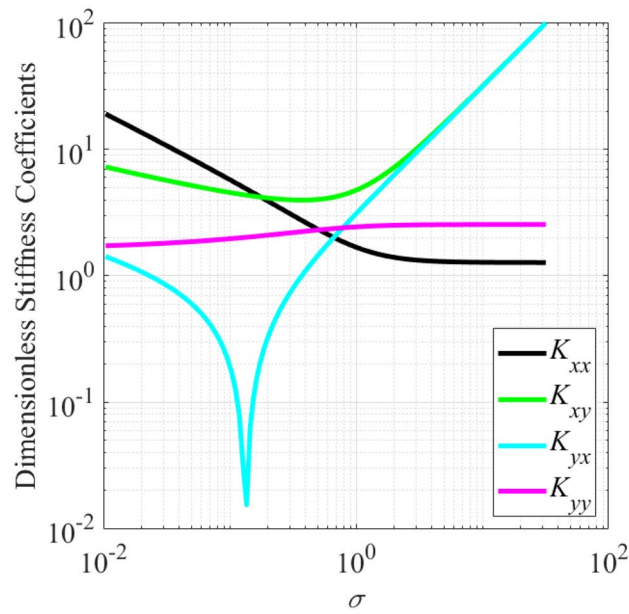
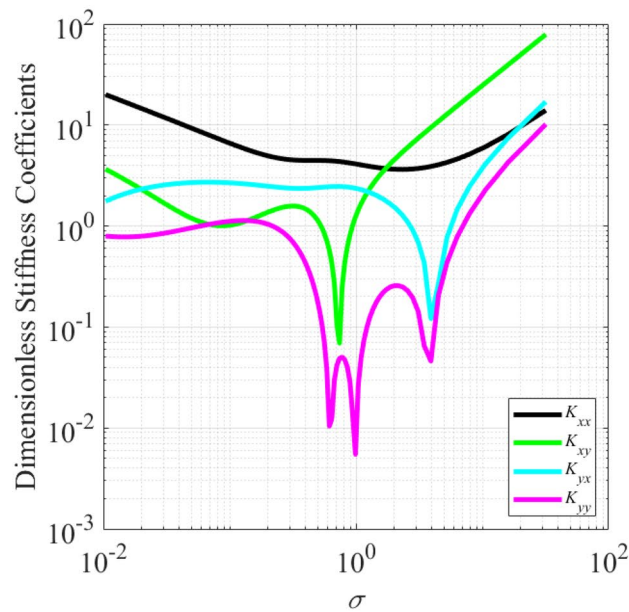


**Figure 3.** Fluid film thickness profile for the case of  $\epsilon_0 = 0.4$  for various wear depth values.



(a)



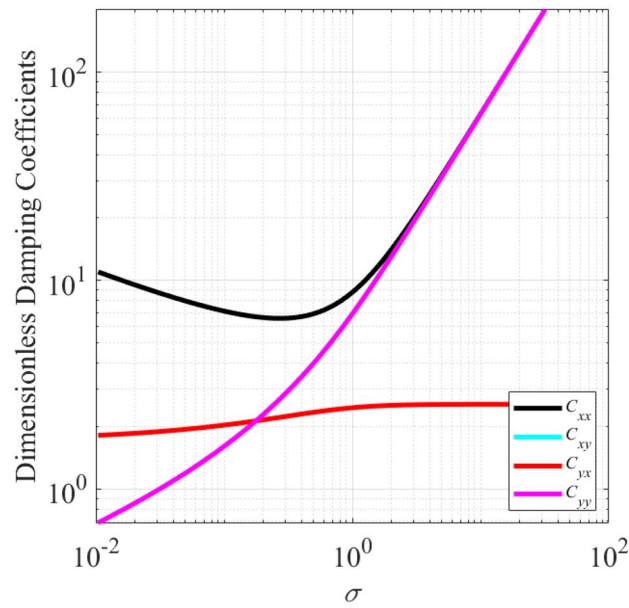
(b)

**Figure 4.** Dimensionless stiffness coefficient as a function of modified Sommerfeld number,  $\sigma$ , for (a) bearing with  $\delta = 0$  (b) bearing with  $\delta = 0.5$ .

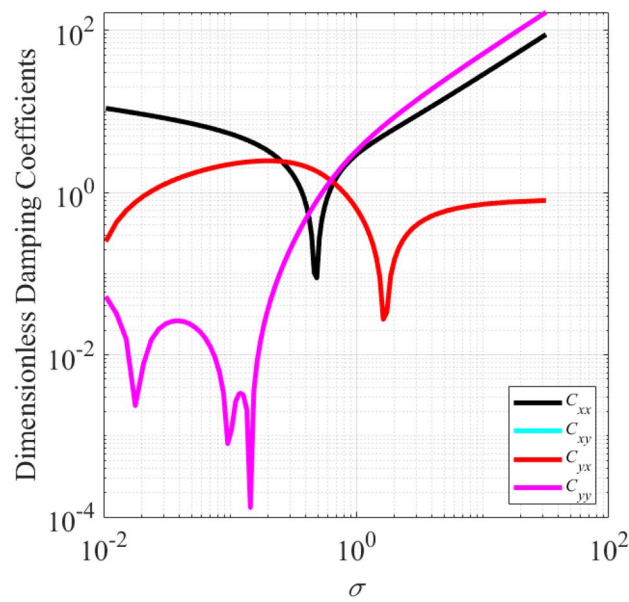
$$K_{yx} = \Delta F_y / \Delta x \tag{37}$$

A net force is produced from the reaction forces resulting from the combination of cross coupled stiffness terms. The net force is tangential to the shaft orbit and follows the direction of the journal’s instantaneous motion. As to produce a forward destabilizing force, the  $K_{xy}$  term must be positive and the  $K_{yx}$  term negative as shown in Fig. 6 for values of  $\delta > 0.05$ . As a result, energy is added to the system and the rotor-bearing system is destabilized by the resultant force from the cross-coupling terms<sup>26</sup>.

The shaft motion within the bearing is usually demonstrated by an elliptical orbit. The area enclosed by the elliptical whirl orbit in the  $X - Y$  plane is represented by the following expression<sup>26</sup>:



(a)



(b)

**Figure 5.** Dimensionless damping coefficient as a function of modified Sommerfeld number,  $\sigma$ , for (a) bearing with  $\delta = 0$  (b) bearing with  $\delta = 0.5$ .

$$A = \pi \bar{x} \bar{y} \sin(\phi_x - \phi_y) \tag{38}$$

where,

$\bar{x}$  is the absolute magnitude of rotor vibration response in the X-direction.

$\bar{y}$  is the absolute magnitude of rotor vibration response in the Y-direction.

$\phi_x$  is the phase angle of vibration response in the X-direction measured counter-clockwise from the X-axis.

$\phi_y$  is the phase angle of vibration response in the Y-direction measured counter-clockwise from the Y-axis.

It is seen that the area can be a positive or negative number with positive being for counter-clockwise whirling and negative for clockwise whirling. The energy input,  $E$ , produced by the bearing coefficients is calculated by integrating the multiplication product of force and displacement around the closed curve of the ellipse. For the cross coupled stiffness coefficients, Zeidan et al.<sup>27</sup> has shown that:

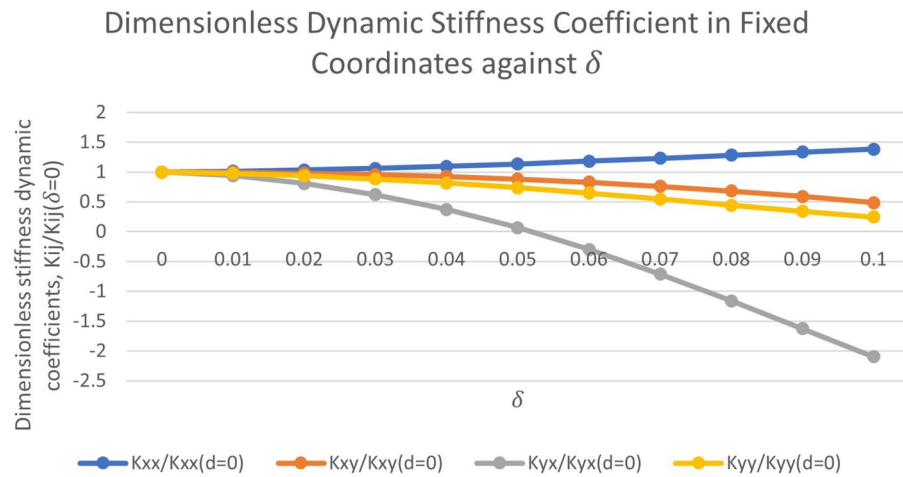


**Figure 6.** Dimensionless dynamic stiffness coefficient in fixed coordinates against  $\delta$  ranging from  $\delta = 0$  to  $\delta = 0.1$ .

$$E = A(K_{xy} - K_{yx}) \quad (39)$$

From Eq. (39), it can be noted that the cross-coupling's destabilizing effect is directly proportional to the area of the whirl orbit and with the net difference between  $K_{xy}$  and  $K_{yx}$ . It is also noted that  $E = 0$ , if  $K_{xy}$  and  $K_{yx}$  are equal and have identical sign. The worst combination is when  $K_{xy}$  and  $K_{yx}$  are equal and opposite in sign which produces a circular orbit<sup>27</sup>. Rotor systems are unique in that  $K_{xy} \neq K_{yx}$  and usually  $K_{xy} > 0, K_{yx} < 0$ <sup>25</sup>. It can be observed in Fig. 6 that  $K_{xy} \neq K_{yx}$  and  $K_{xy} > 0$  for values of  $\delta = 0$  to  $\delta = 0.1$ . It is also noted that, when  $\delta \leq 0.05$ ,  $K_{xy}$  and  $K_{yx}$  have the same positive sign and when  $\delta > 0.05$ ,  $K_{xy}$  remain positive whereas  $K_{yx}$  became negative which makes the net difference between  $K_{xy}$  and  $K_{yx}$  larger for  $\delta > 0.05$  as compared to when  $\delta \leq 0.05$ . A larger net difference between  $K_{xy}$  and  $K_{yx}$  contributes to a larger energy input as per Eq. (39). Also, when the signs are the same, the cross-coupling has the effect of increasing the apparent asymmetry in  $K_{xx}$  and  $K_{yy}$ <sup>26</sup>. Thus, it can be deduced that when  $\delta \leq 0.05$  the apparent asymmetry in  $K_{xx}$  and  $K_{yy}$  increases (rotor-bearing system becomes more stable) whereas when  $\delta > 0.05$  the apparent asymmetry in  $K_{xx}$  and  $K_{yy}$  decreases (rotor-bearing system becomes more unstable).

He et al.<sup>25</sup> mentioned that large asymmetry of  $K_{xx}$  and  $K_{yy}$  is the main cause of split critical speeds and non-circular (elliptical) orbit shapes. Incorporating asymmetry into the direct stiffnesses has the well-known effect of producing flat, elongated whirl orbits in the vertical and horizontal direction. This reduces the area of the orbit and thereby lessens the energy input by cross-coupled stiffness. Sufficient asymmetry flattens the orbit completely to a straight line, and the unstable system is rendered stable as the energy input becomes zero<sup>26</sup>.

Figure 7 shows the dimensionless damping dynamic coefficient against  $\delta$  for values of  $\delta = 0$  to  $\delta = 0.5$  when the rotor is operated under high operating regime ( $\epsilon = 0.61$ ). It is observed that  $C_{xx}$  decreases by 17.38 %,  $C_{xy}$  decreases by 69.10 %,  $C_{yx}$  decreases by 69.10 %, and  $C_{yy}$  decreases by 37.78 %.

Damping, which is generally assumed to be positive, dissipates energy from the dynamic motion of the rotor-bearing system and thus promotes stability. The direct damping coefficient is related to the change in force due to a small change in velocity as shown in Eqs. (40) and (41)<sup>25</sup>.

$$C_{xx} = \Delta F_x / \Delta \dot{x} \quad (40)$$

$$C_{yy} = \Delta F_y / \Delta \dot{y} \quad (41)$$

Due to the rotor's whirling motion, the combination of the two direct damping coefficients,  $C_{xx}$  and  $C_{yy}$  produces a force that is tangential to the vibration orbit. This direct damping force acts against the whirling motion, helping to retard or slow it<sup>25</sup>. As for cross-coupled damping, it is often found that the effect of cross-coupled stiffness outweighs the effect of cross-coupled damping. This is because the resulting energy from cross-coupled damping is identically zero. Hence, in the absence of cross-coupled stiffness, cross-coupled damping cannot drive the rotor-bearing system unstable by itself<sup>26</sup>. It can be concluded that in general, the effect of wear on the dynamic coefficients of journal bearings is such that the dynamic coefficients except for  $K_{xx}$  decrease with increasing  $\delta$ . This result is consistent with the work of Zeidan & Herbage<sup>27</sup>.

### Effect of wear on the vibration response of the rotor

The numerical simulation to study the effect of wear on the vibration response of the rotor was undertaken for 3 different loaded operating regime namely low loaded operating regime ( $0.1 \leq \epsilon_0 \leq 0.2$ ), moderately loaded operating regime ( $0.3 \leq \epsilon_0 \leq 0.5$ ) and highly loaded operating regime ( $0.6 \leq \epsilon_0 \leq 0.75$ )<sup>28</sup>. The unbalance parameter

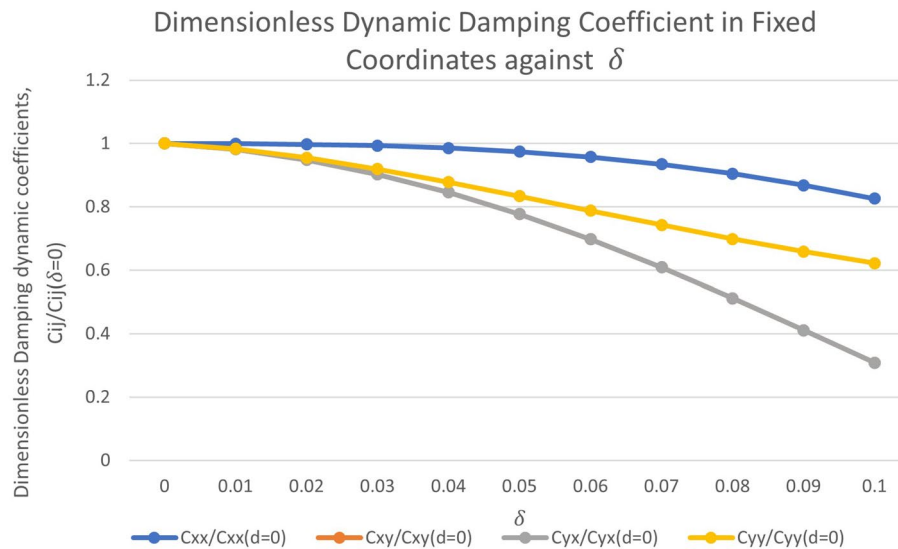


**Figure 7.** Dimensionless dynamic damping coefficient in fixed coordinates against  $\delta$  ranging from  $\delta = 0$  to  $\delta = 0.1$ .

$u$  was set at 0.05. The dimensionless journal mass  $m$  was varied from 2 to 73. The wear depth parameter ratio  $\delta$  was varied from 0 to 0.5 and the results are presented for  $\delta$  increments of 0.1.

#### Low loaded operating regime ( $0.1 \leq \epsilon_0 \leq 0.2$ )

The effect of wear on the vibration response of rotor when the rotor is operated under low loaded operating regime ( $\epsilon_0 = 0.1$ ) whereby  $m = 2$  is shown from Fig. 8 to Fig. 10. Figure 8 shows the rotor whirl orbit for low loaded operating regime ( $\epsilon_0 = 0.1$ ); (a) with a boundary view of unit circle (b) enlarged view. Figure 8a and b show that the rotor whirl orbit increases in size with increasing  $\delta$ . Figure 9 shows the vibration response in the X-direction for low loaded operating regime ( $\epsilon_0 = 0.1$ ) for (a)  $\delta = 0$  (b)  $\delta = 0.5$ . The magnitude of X response has increased from 0.018 in Fig. 9a to 0.046 in Fig. 9b which yields a net increase of 161% when  $\delta$  increases from  $\delta = 0$  to  $\delta = 0.5$ . Figure 10 shows the vibration response in the Y-direction for low loaded operating regime ( $\epsilon_0 = 0.1$ ) for (a)  $\delta = 0$  (b)  $\delta = 0.5$ . The magnitude of Y has increased from 0.006 in Fig. 10a to 0.018 in Fig. 10b which yields a net increase of 179% when  $\delta$  increases from  $\delta = 0$  to  $\delta = 0.5$ .

#### Moderately loaded operating regime ( $0.3 \leq \epsilon_0 \leq 0.5$ )

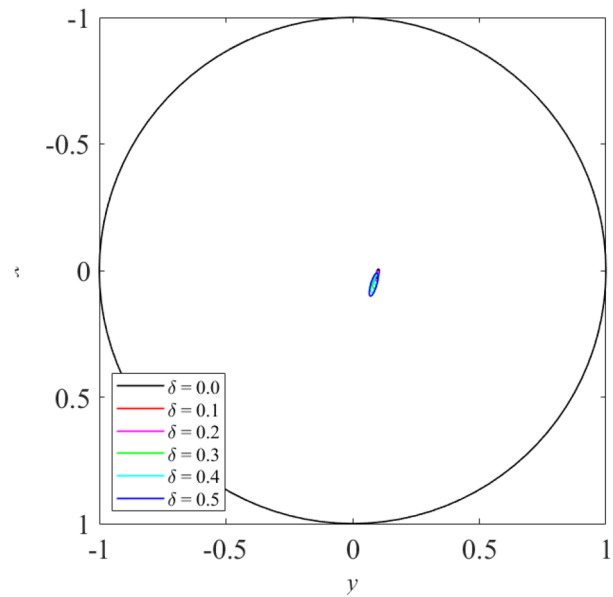
When the rotor is operated under moderately loaded operating regime ( $\epsilon_0 = 0.4$ ) whereby  $m = 12.5$ , the effect of wear on the vibration response of rotor can be seen in Figs. 11, 12 and 13. Figure 11 shows the rotor whirl orbit for moderately loaded operating regime ( $\epsilon_0 = 0.4$ ); (a) with a boundary view of unit circle (b) enlarged view. Figure 11a and b show that the rotor whirl orbit increases in size with increasing  $\delta$ . Figure 12 shows the vibration response in the X-direction for moderately loaded operating regime ( $\epsilon_0 = 0.4$ ) for (a)  $\delta = 0$  (b)  $\delta = 0.5$ . The magnitude of X response increased from 0.056 in Fig. 12a to 0.154 in Fig. 12b, which gives a net increase of 176% when  $\delta$  increases from  $\delta = 0$  to  $\delta = 0.5$ . Figure 13 shows the vibration response in the Y-direction for moderately loaded operating regime ( $\epsilon_0 = 0.4$ ) for (a)  $\delta = 0$  (b)  $\delta = 0.5$ . The magnitude of Y response increased from 0.031 in Fig. 13a to 0.037 in Fig. 13b which yields a net increase of 20.4% when  $\delta$  increases from  $\delta = 0$  to  $\delta = 0.5$ .

#### Highly loaded operating regime ( $0.6 \leq \epsilon_0 \leq 0.75$ )

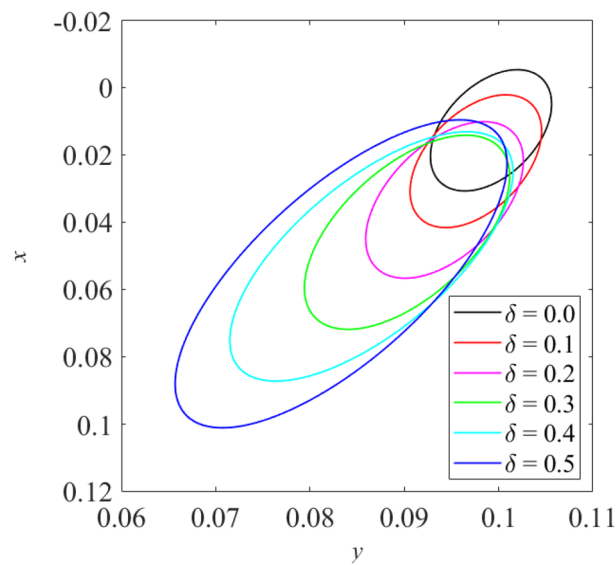
The effect of wear on the vibration response of rotor when the rotor is operated under highly loaded operating regime ( $\epsilon_0 = 0.75$ ) whereby  $m = 73$  is observed in Figs. 14, 15 and 16. Figure 14 shows the rotor whirl orbit for highly loaded operating regime ( $\epsilon_0 = 0.75$ ); (a) with a boundary view of unit circle (b) enlarged view. Figure 14a and b show that the rotor whirl orbit increases in size with increasing  $\delta$ . Figure 15 shows the vibration response in the X-direction for highly loaded operating regime ( $\epsilon_0 = 0.75$ ) for (a)  $\delta = 0$  (b)  $\delta = 0.5$ . The magnitude of X response increased from 0.059 in Fig. 15a to 0.443 in Fig. 15b which yields a net increase of 650.8% when  $\delta$  increases from  $\delta = 0$  to  $\delta = 0.5$ . Figure 16 shows the vibration response in the Y-direction for highly loaded operating regime ( $\epsilon_0 = 0.75$ ) for (a)  $\delta = 0$  (b)  $\delta = 0.5$ . The magnitude of Y response dropped from 0.059 in Fig. 16a to 0.035 in Fig. 16b which yields a net drop of 41.0% when  $\delta$  increases from  $\delta = 0$  to  $\delta = 0.5$ .

In general, the effect of wear on the vibration response of the rotor is such that when  $\delta$  increases, the vibration response of the rotor in the X- and Y-direction under all 3 loaded operating regime increases with the exception of the response in the Y-direction for the highly loaded operating regime. For a constant value of  $\epsilon_0$ ,  $\varphi_0$  decreases as  $\delta$  increases from  $\delta = 0$  to  $\delta = 0.5$ . This means that the rotor is moving closer to the vertical axis and when  $\delta$  increases, the fluid-film thickness increases. As the fluid-film thickness increases, the dynamic stiffness reduces and when subjected to the same unbalance force, the amplitude of the rotor's displacement increases. However, the vibration response of the rotor in Y-direction when the rotor is operating under highly loaded operating





(a)



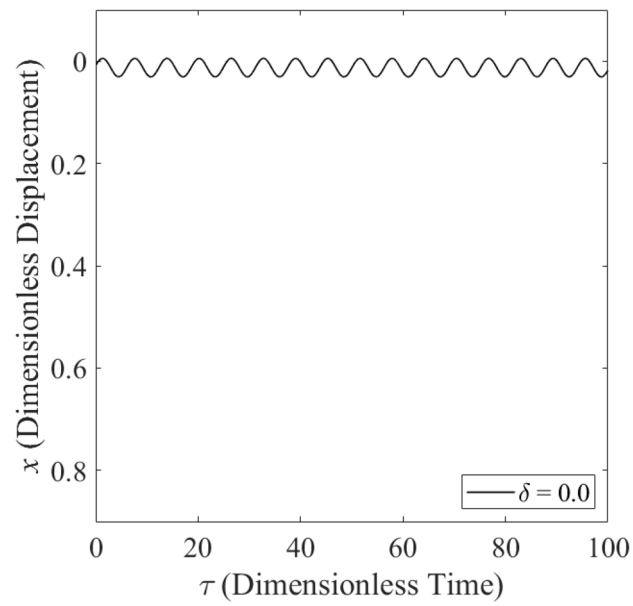
(b)

**Figure 8.** Rotor whirl orbit for low loaded operating regime ( $\epsilon_0 = 0.1$ ) (a) with a boundary view of unit circle (b) enlarged view.

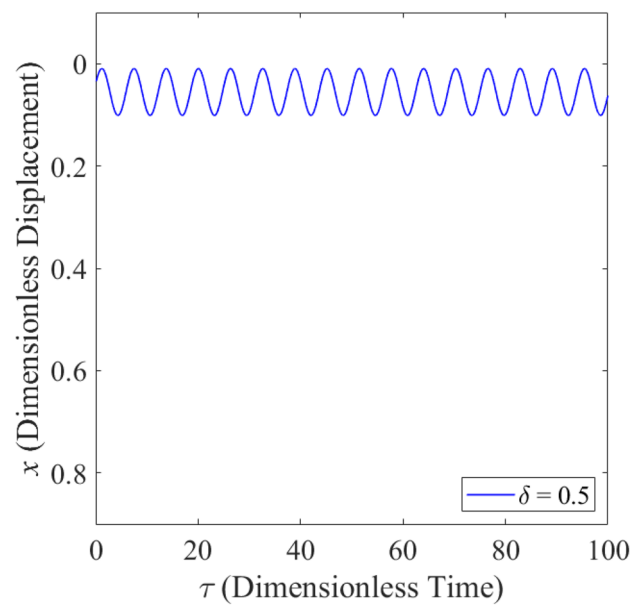
regime decreases with increasing  $\delta$ . This is because as  $\delta$  increases, the clearance and fluid-film thickness in the Y-direction reduces. As such, the dynamic stiffness in that direction increases and when subjected to the same unbalance force, the amplitude of the rotor's displacement reduces as  $\delta$  is increased from 0 to 0.5.

### Conclusion

The effect of wear in journal bearings on the behavior of a rigid rotor, particularly on the static equilibrium position, the dynamic coefficients, and the vibration response of the rotor was investigated. The effect of wear on the static equilibrium position of the rotor was examined for values of  $\epsilon_0$  between 0.1 and 0.9 with  $\delta$  varied from 0 to 0.5, in increments of 0.1. The results showed that  $\epsilon_0$  has an inverse relationship with  $\varphi_0$ , where increase in the value of  $\epsilon_0$  cause the value of  $\varphi_0$  to decrease. The effect of wear on the dynamic coefficients of journal bearings was investigated for values of  $\epsilon_0$  between 0.1 and 0.75 with  $\delta$  varied from 0 to 0.5. The numerical results showed that

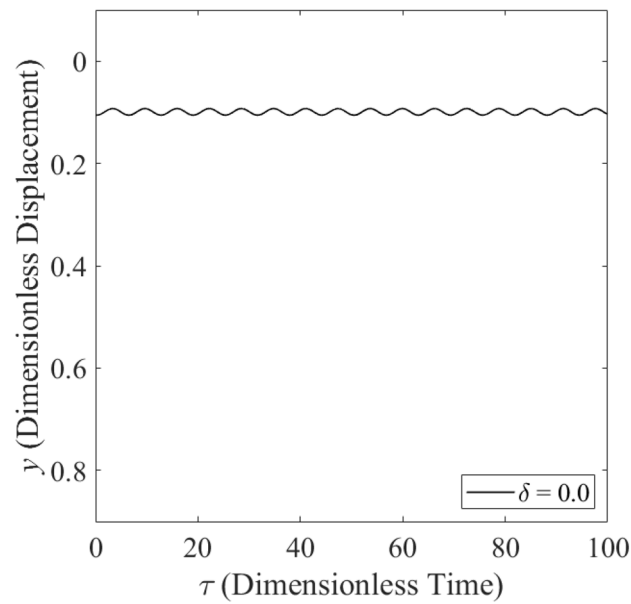


(a)

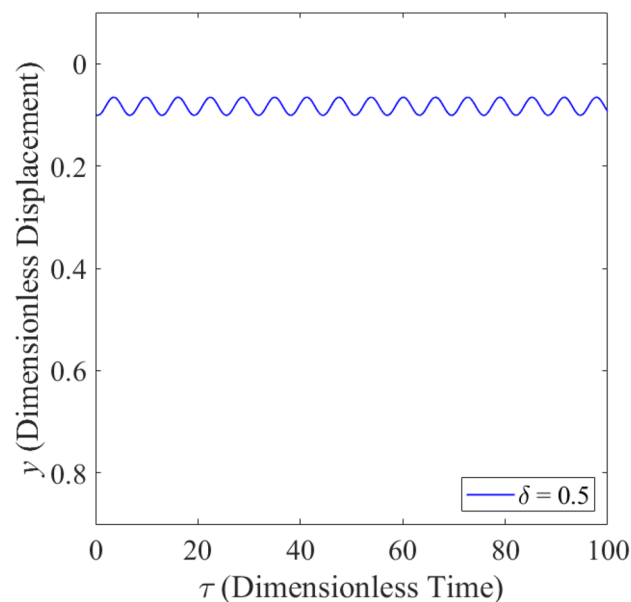


(b)

**Figure 9.** Vibration response in the X-direction for low loaded operating regime ( $\epsilon_0 = 0.1$ ) for (a)  $\delta = 0$  (b)  $\delta = 0.5$ .



(a)

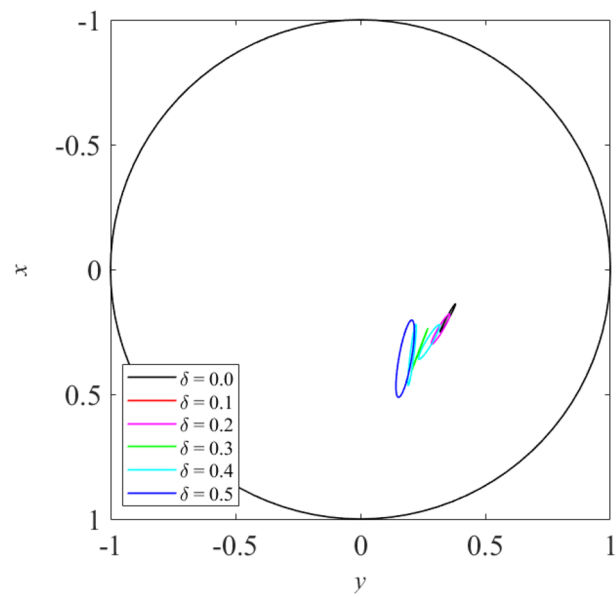


(b)

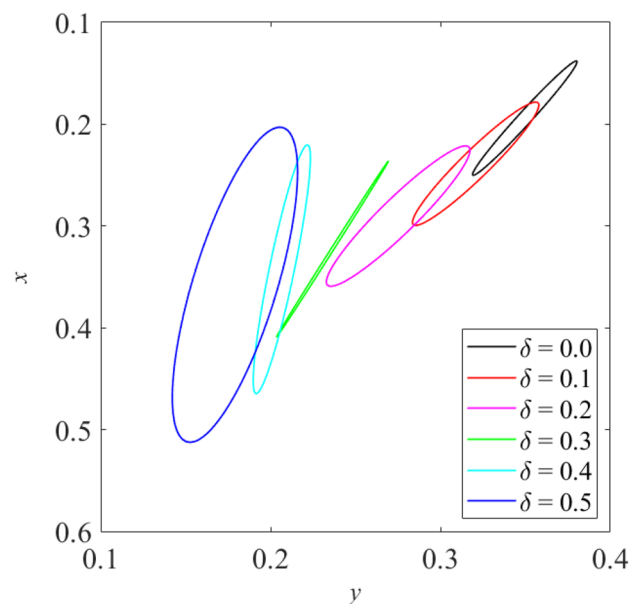
**Figure 10.** Vibration response in the Y-direction for low loaded operating regime ( $\epsilon_0 = 0.1$ ) for (a)  $\delta = 0$  (b)  $\delta = 0.5$ .

the dynamic coefficients, except for  $K_{xx}$ , decrease with increasing  $\delta$ . The effect of wear on the vibration response of a rigid rotor was undertaken for three different operating regimes of the journal bearings, namely low loaded operating regime, moderately loaded operating regime and highly loaded operating regime. The unbalance parameter  $u$  was set at 0.05. The dimensionless journal mass  $m$  was varied from 2 to 73.  $\delta$  was varied from 0 to 0.5 in increments of 0.1. The numerical results showed that increasing the wear depth in the journal bearings generally caused an increase in the vibration response amplitude of the rigid rotor in the X- and Y-directions, for all three cases of operating regimes, with the exception of the response amplitude of the rotor in the Y-direction for the highly loaded operating regime.



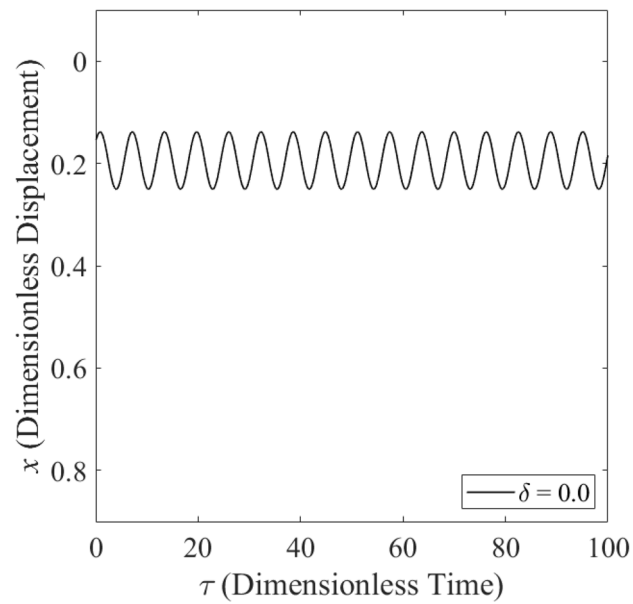


(a)

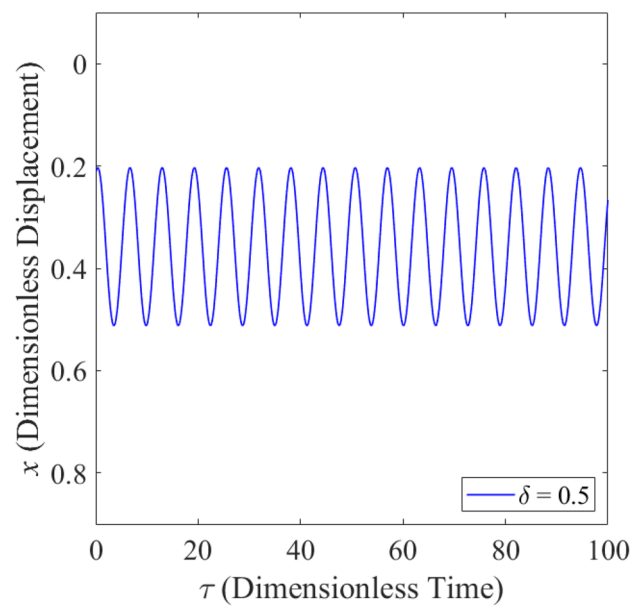


(b)

**Figure 11.** Rotor whirl orbit for moderately loaded operating regime ( $\epsilon_0 = 0.4$ ) (a) with a boundary view of unit circle (b) enlarged view.

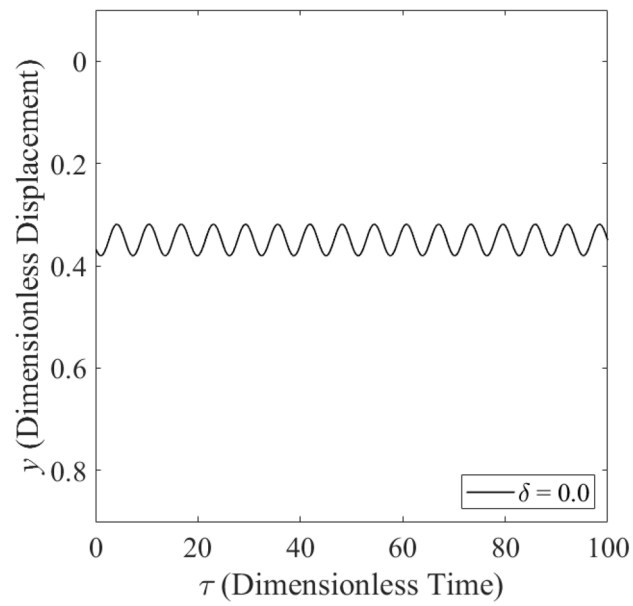


(a)

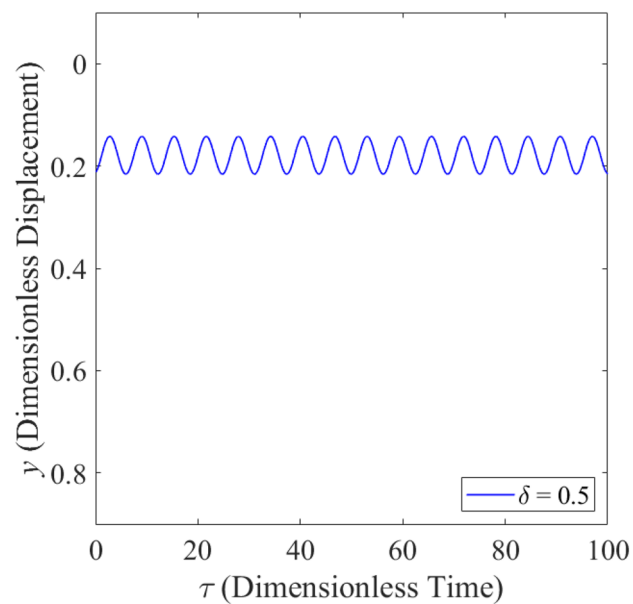


(b)

**Figure 12.** Vibration response in the X-direction for moderately loaded operating regime ( $\epsilon_0 = 0.4$ ) for (a)  $\delta = 0$  (b)  $\delta = 0.5$ .

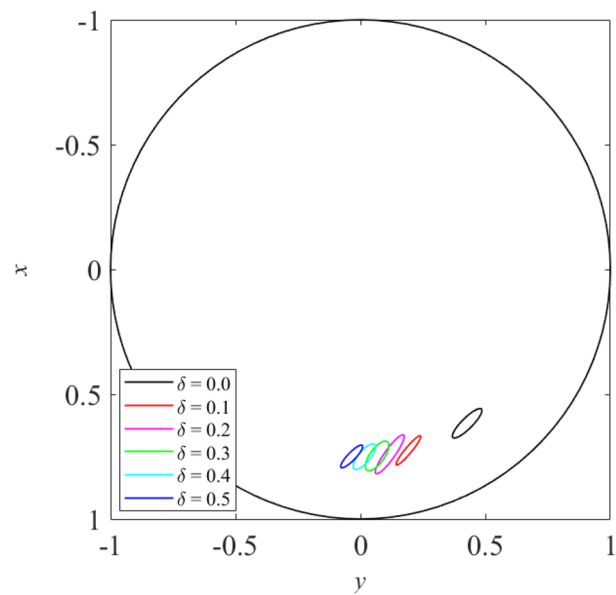


(a)

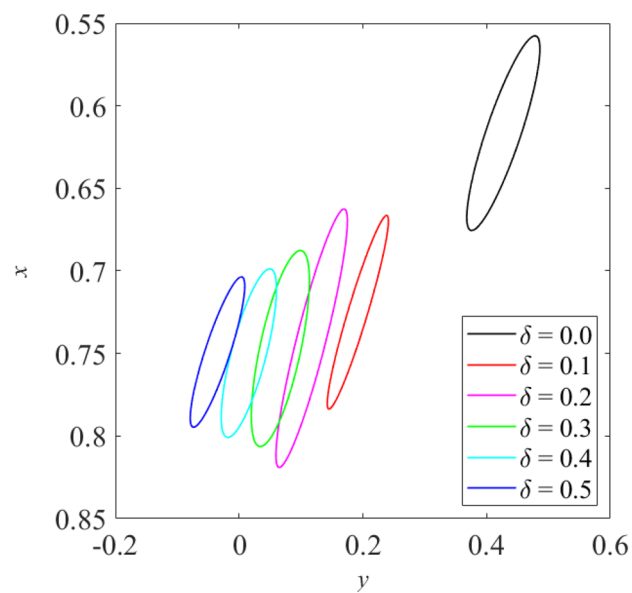


(b)

**Figure 13.** Vibration response in the Y-direction for moderately loaded operating regime ( $\epsilon_0 = 0.4$ ) for (a)  $\delta = 0$  (b)  $\delta = 0.5$ .

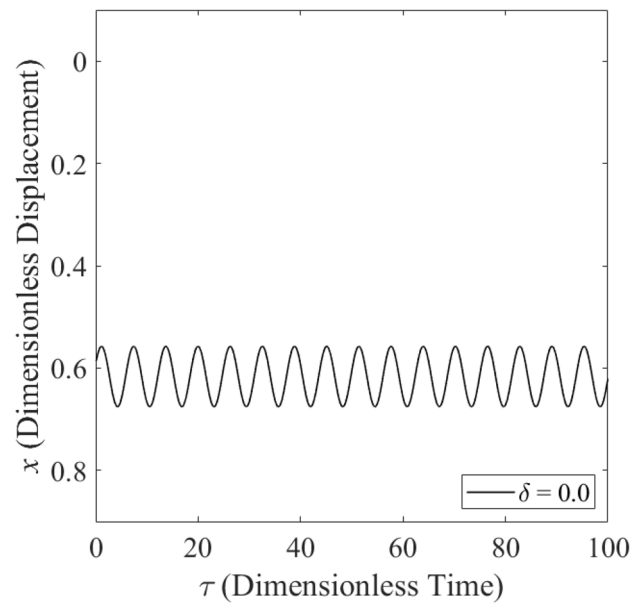


(a)

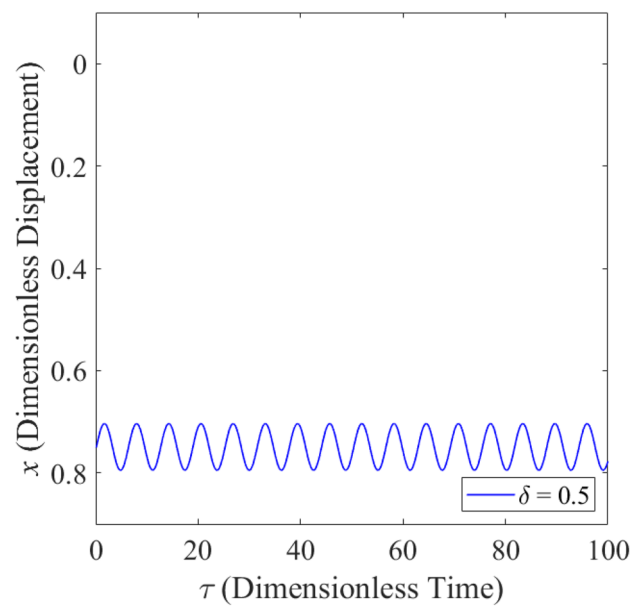


(b)

**Figure 14.** Rotor whirl orbit for highly loaded operating regime ( $\epsilon_0 = 0.75$ ) (a) with a boundary view of unit circle (b) enlarged view.

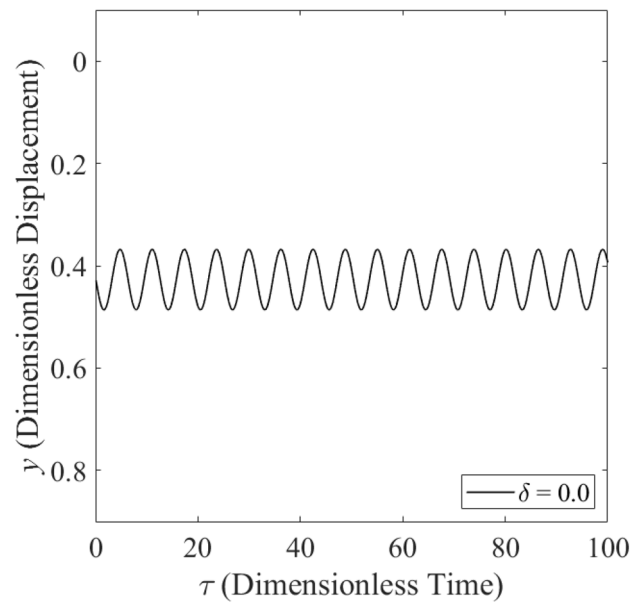


(a)

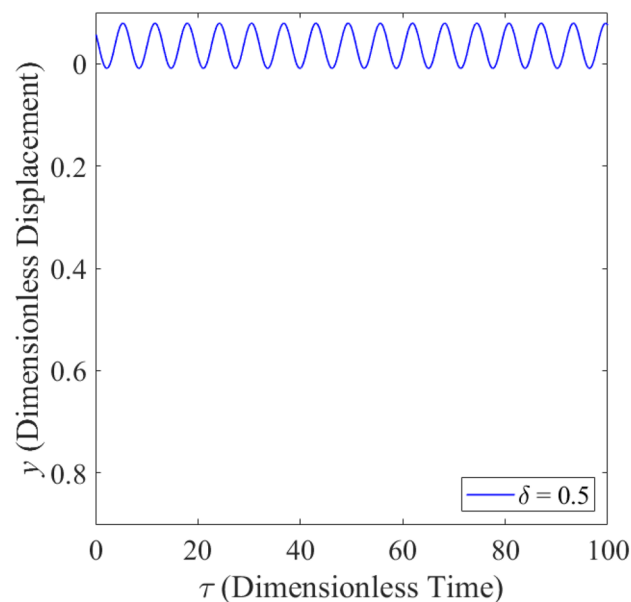


(b)

**Figure 15.** Vibration response in the X-direction for highly loaded operating regime ( $\epsilon_0 = 0.75$ ) for (a)  $\delta = 0$  (b)  $\delta = 0.5$ .



(a)



(b)

**Figure 16.** Vibration response in the Y-direction for highly loaded operating regime ( $\epsilon_0 = 0.75$ ) for (a)  $\delta = 0$  (b)  $\delta = 0.5$ .

#### Data availability

The datasets generated and/or analyzed during the current study are available from the corresponding author upon reasonable request.

#### Code availability

The code generated during the current study are available from the corresponding author upon reasonable request.

Received: 11 January 2024; Accepted: 23 April 2024

Published online: 30 April 2024

## References

1. Hashimoto, H. Optimization of oil flow rate and oil film temperature rise in high speed hydrodynamic journal bearings. In *Tribology Series: Tribology for Energy Conservation* Vol. 34 205–210 (Elsevier, 1998).
2. Machado, T. H. & Cavalca, K. L. Geometric discontinuities identification in hydrodynamic bearing. In *Proceedings of the 9th IFToMM International Conference on Rotor Dynamics*, vol. 21. 895–908 (Springer, 2015).
3. Sharma, S. & Awasthi, R. K. Performance of hydrodynamic journal bearing operating under transient wear. *Mech. Mech. Eng.* **22**(1), 153–170 (2018).
4. Machado, T. H., Alves, D. S. & Cavalca, K. L. Investigation about journal bearing wear effect on rotating system dynamic response in time domain. *Tribol. Int.* **129**, 124–136 (2019).
5. Papanikolaou, M. G., Farmakopoulos, M. G. & Papadopoulos, C. A. Alternation of the dynamic coefficients of short journal bearings due to wear. *Int. J. Struct. Integr.* **6**(5), 649–664 (2015).
6. Viana, C. A. A., Alves, D. S. & Machado, T. H. Linear and nonlinear performance analysis of hydrodynamic journal bearings with different geometries. *Appl. Sci.* **12**(7), 3215 (2022).
7. Childs, D. *Turbomachinery Rotordynamics: Phenomena, Modeling, and Analysis* (Wiley, 1993).
8. Ishida, Y. & Yamamoto, T. *Linear and Nonlinear Rotordynamics: A Modern Treatment with Applications* (Wiley, 2013).
9. Turaga, R., Sekhar, A. S. & Majumdar, B. C. Stability analysis of a rigid rotor supported on hydrodynamic journal bearings with rough surfaces using the stochastic finite element method. *Proc. Inst. Mech. Eng. Part J: J. Eng. Tribol.* **212**(2), 121–130 (1998).
10. Rao, T. & Sawicki, J. T. Linear stability analysis for a hydrodynamic journal bearing considering cavitation effects. *Tribol. Trans.* **45**(4), 450–456 (2002).
11. Hirani, H., Athre, K. & Biswas, S. Rapid and globally convergent method for dynamically loaded journal bearing design. *Proc. Inst. Mech. Eng. Part J: J. Eng. Tribol.* **212**(3), 207–214 (1998).
12. Mokhtar, M., Howarth, R. & Davies, P. Wear characteristics of plain hydrodynamic journal bearings during repeated starting and stopping. *ASLE Trans.* **20**(3), 191–194 (1977).
13. Dufrane, K., Kannel, J. & McCloskey, T. Wear of steam turbine journal bearings at low operating speeds. *J. Lubr. Technol.* **105**(2), 313–317 (1983).
14. Fillon, M. & Bouyer, J. Thermohydrodynamic analysis of a worn plain journal bearing. *Tribol. Int.* **37**(2), 129–136 (2004).
15. Bouyer, J., Fillon, M. & Pierre-Danos, I. Influence of wear on the behavior of a two-lobe hydrodynamic journal bearing subjected to numerous startups and stops. *Tribol. Int.* **129**, 205–208 (2007).
16. Machado, T. H. & Cavalca, K. L. Evaluation of hydrodynamic bearings with geometric discontinuities. In *Proceedings of the 21st Brazilian Congress of Mechanical Engineering*, Natal, RN, Brazil (2011).
17. Chasalevris, A. C., Nikolakopoulos, P. G. & Papadopoulos, C. A. Dynamic effect of bearing wear on rotor-bearing system response. *J. Vib. Acoust.* **135**(1), 011008 (2013).
18. Chasalevris, A., Dohnal, F. & Chatzisavvas, I. Experimental detection of additional harmonics due to wear in journal bearings using excitation from a magnetic bearing. *Tribol. Int.* **71**(1), 158–167 (2014).
19. Machado, T. H. & Cavalca, K. L. Modeling of hydrodynamic bearing wear in rotor-bearing systems. *Mech. Res. Commun.* **69**, 15–23 (2015).
20. Jamil, A. N., Ali, A. A. H. & Mohammed, T. Study the dynamic behavior of rotor supported on a worn journal bearings. *J. Eng.* **21**(12), 1–18 (2015).
21. Kim, S., Shin, D. & Palazzolo, A. B. A review of journal bearing induced nonlinear rotordynamic vibrations. *J. Tribol.* **143**(11), 111802 (2021).
22. San Andrés, L. Hydrodynamic fluid film bearings and their effect on the stability of rotating machinery. In *Design and Analysis of High Speed Pumps; Educational Notes RTO-EN-AVT-143, Paper 10; RTO: Neuilly-sur-Seine, France*, 10-1-10-36 (2006).
23. Lund, J. W. & Saibel, E. Oil whip whirl orbits of a rotor in sleeve bearings. *J. Eng. Ind.* **89**(4), 813–823 (1967).
24. Gertzos, K., Nikolakopoulos, P., Chasalevris, A. & Papadopoulos, C. Wear identification in rotor-bearing systems by measurements of dynamic bearing characteristics. *Comput. Struct.* **89**(1–2), 55–66 (2011).
25. He, M., Cloud, C. H., Byrne, J. M. & Vázquez, J. A. Fundamentals of fluid film journal bearing operation and modeling. In *Asia Turbomachinery & Pump Symposium. 2016 Proceedings. (2016). Turbomachinery Laboratories, Texas A & M Engineering Experiment Station.*
26. Murphy, B. T. Eigenvalues of Rotating Machinery. Ph. D. Dissertation, *Texas A & M University* (College Station, Texas, USA, 1984).
27. Zeidan, F. Y. & Herbage, B. S. Fluid film bearing fundamentals and failure analysis. In *Proceedings of the 20th Turbomachinery Symposium (1991)*. Texas A & M University. Turbomachinery Laboratories
28. Zakaria, A. A. & Inayat-Hussain, J. I. Bifurcation analysis of rigid rotor supported by nonlinear journal bearing. In *2nd International Conference on Mechanical, Automotive and Aerospace Engineering (ICMAAE 2013)*, Selangor, Malaysia (2013).

## Acknowledgements

This work was supported by Tenaga Nasional Berhad (TNB) and UNITEN through the BOLD 2023 Research Grant under the project code of J510050949. The first author would also like to express his sincere gratitude to Universiti Tenaga Nasional for awarding him the UNITEN-YCU Postgraduate Scholarship to support his studies.

## Author contributions

The authors contributed equally to this work and approved it for publication.

## Funding

This work was supported by Tenaga Nasional Berhad (TNB) and UNITEN through the BOLD 2023 Research Grant under the project code of J510050949.

## Competing interests

The authors declare no competing interests.

## Additional information

**Correspondence** and requests for materials should be addressed to J.I.I.-H.

**Reprints and permissions information** is available at [www.nature.com/reprints](http://www.nature.com/reprints).

**Publisher's note** Springer Nature remains neutral with regard to jurisdictional claims in published maps and institutional affiliations.



**Open Access** This article is licensed under a Creative Commons Attribution 4.0 International License, which permits use, sharing, adaptation, distribution and reproduction in any medium or format, as long as you give appropriate credit to the original author(s) and the source, provide a link to the Creative Commons licence, and indicate if changes were made. The images or other third party material in this article are included in the article's Creative Commons licence, unless indicated otherwise in a credit line to the material. If material is not included in the article's Creative Commons licence and your intended use is not permitted by statutory regulation or exceeds the permitted use, you will need to obtain permission directly from the copyright holder. To view a copy of this licence, visit <http://creativecommons.org/licenses/by/4.0/>.

© The Author(s) 2024